



## Biosorption of $Pb^{2+}$ , $Ni^{2+}$ and $Cu^{2+}$ ions from aqueous solutions by L-cystein-modified montmorillonite-immobilized alginate nanocomposite

Alok Mittal<sup>a,\*</sup>, Rais Ahmad<sup>b</sup>, Imran Hasan<sup>b</sup>

<sup>a</sup>Department of Chemistry, Maulana Azad National Institute of Technology, Bhopal 462003, India, Tel. +91 9425025427; Fax: +91 755 2670562; email: [aljmittal@yahoo.co.in](mailto:aljmittal@yahoo.co.in)

<sup>b</sup>Environmental Research Laboratory, Department of Applied Chemistry, Aligarh Muslim University, Aligarh 202002, India, Tel. +91 0571 2700920 23, ext. 3000; Fax: +91 0571 2400528; emails: [rais45@rediffmail.com](mailto:rais45@rediffmail.com) (R. Ahmad), [imranhasan98@gmail.com](mailto:imranhasan98@gmail.com) (I. Hasan)

Received 13 July 2015; Accepted 21 August 2015

### ABSTRACT

In this study, L-cystein-modified montmorillonite (MMT)-immobilized sodium alginate biopolymer-based nanocomposite was synthesized using solution casting method. The synthesized material was characterized by X-ray diffraction, FTIR, TGA-DTG, scanning electron microscopy and transmission electron microscopy techniques. The material was further evaluated for the removal of heavy metal ions like ( $Pb^{2+}$ ,  $Ni^{2+}$  and  $Cu^{2+}$ ) from aqueous solutions. The effect of various parameters such as pH, agitation time, initial metal ion concentration, temperature and adsorbent dose on the extent of adsorption was investigated. The equilibrium data obtained by experiments were well analysed by four isotherm models, and the results are well fitted with Langmuir model at 50°C, and a maximum adsorption capacity ( $q_m$ ) 100.00, 111.11 and 125.00 ( $mg\ g^{-1}$ ) was obtained for  $Cu^{2+}$ ,  $Pb^{2+}$  and  $Ni^{2+}$ , respectively. Various kinetic equations were applied to kinetic data, and the results are best found to follow pseudo-second-order kinetic model. Thermodynamic parameters of the adsorption process such as the standard Gibbs free energy change ( $\Delta G^\circ$ ), standard enthalpy change ( $\Delta H^\circ$ ), standard entropy change ( $\Delta S^\circ$ ) were calculated, and the result showed that adsorption of heavy metals onto Alg-Cys-MMT is spontaneous and endothermic in nature.

*Keywords:* Amino acid; Adsorption; Nanocomposite; TGA; Isotherm; Heavy metals

### 1. Introduction

Pollution by heavy metals due to their non-biodegradable properties and toxicity is currently of great concern due to its serious environmental impact [1]. Heavy metals are not only potential threat to air, water and soil but also accumulate throughout the food chain and finally affect human beings [2]. These

heavy metals ions are found in various industrial sources such as electroplating, textile, metal finishing, chemical manufacturing and storage batteries [3].

Conventional techniques for the removal of heavy metal ions from aqueous solutions include ion exchange, chemical precipitation, evaporation, membrane filtration, reverse osmosis, electrodialysis and adsorption [4]. Among these techniques, adsorption is generally regarded as an effective and economical

\*Corresponding author.

method for wastewater treatment. A selective property is the main advantage of adsorbent for the removal of metal ions which depend on the functional groups on their surface such as thiol, amine, amides, carboxylic acid, hydroxyl groups [5,6].

Extensive efforts have recently been made towards the development of biopolymer (chitosan, chitin, starch, cellulose, sodium alginate, etc.)-based nanocomposites that show higher affinity for heavy metal ion removal than synthetic polymer-based nanocomposite [7,8]. Among these biopolymers, alginate is the most widely studied biopolymer which is a natural polysaccharide consists of linear copolymers composed of  $\beta$ -D-mannuronate (M) and  $\alpha$ -L-guluronate (G) linked by  $\alpha$ -1,4-glycosidic bonds [9]. Besides a lot of advantages, biopolymers suffer some serious drawbacks like poor mechanical strength, water solubility and lack of reusability, but it is possible to overcome these drawbacks and control the stability and solubility by the introduction the nanoparticles within the matrix [10].

In various types of smectites minerals, montmorillonite (MMT) is the most important and widely used phyllosilicate as the filler in polymer nanocomposites [11,12]. Their specific characteristics like large active surface area, ion exchange capacity and ability to swell remarkably in water improve functional properties and mechanical properties of nanocomposites [13,14]. Single amino acid molecule could hold certain advantages as pseudo-affinity ligands for industrial application [15]. Immobilization of MMT by natural amino acid L-cystein which interacts through its carboxyl, amino and thiol groups around their isoelectronic point leads to an increase of interlayer gallery of MMT which can be reinforced into biopolymer matrix leading to the formation of a nanocomposite which shows a higher adsorption capacity as compared to pure alginate and MMT.

In the present work, we describe the synthesis and characterization of L-cystein-immobilized MMT sodium alginate nanocomposite adsorbent by solvent casting process. The adsorbent was characterized by X-ray diffraction (XRD), FTIR, scanning electron microscopy (SEM), transmission electron microscopy (TEM) and TGA-DSC analysis. The adsorbent was evaluated for the removal of toxic heavy metal ions ( $\text{Pb}^{2+}$ ,  $\text{Ni}^{2+}$  and  $\text{Cu}^{2+}$ ) from the aqueous solutions.

## 2. Experimental

### 2.1. Materials and methods

Sodium alginate (laboratory grade) and MMT K10 powder used in this study were supplied from

Sigma-Aldrich (India), and L-cystein hydrochloride was purchased from CDH (India). NaOH (97%) was purchased from Fischer Scientific (Mumbai, India), and HCl (35%) was purchased from Merck, India. Nitrate salts of  $\text{Cu}^{2+}$ ,  $\text{Pb}^{2+}$  and  $\text{Ni}^{2+}$  were also purchased from Merck, India. All the chemicals were used as received without any further purification. The stock solutions of metal ions were prepared by dissolving an appropriately weighed amount of nitrate salts of  $\text{Cu}^{2+}$ ,  $\text{Pb}^{2+}$  and  $\text{Ni}^{2+}$  in double-distilled water.

### 2.2. Immobilization of MMT with L-cystein

Cation exchange process was used for the immobilization of nanoclay material by L-cystein [16]. MMT (5 g) interacted at 60°C with a 100-mL solution containing 0.1 M L-cystein for about 48 h. A washing procedure was applied after binding procedure to remove the any possible unreacted L-cystein from the Cys-MMT which was filtered and resuspended in deionized water. The suspension was stirred for about 1 h at room temperature, and the clay was separated by filtration. The modified clay was washed several times with deionized water using the same procedure. Then, Cys-MMT clay was dried with vacuum oven at 60°C and stored for further use.

### 2.3. Synthesis of Alg-Cys-MMT nanocomposite

The nanocomposite material was synthesized by solvent casting method reported elsewhere [17]. A specific amount of MMT (1, 3 and 5% w/w on solid sodium alginate) was dispersed in 100 mL of distilled water and vigorously stirred for 24 h at room temperature. Afterwards, the alginate (5 g) was taken with 200 mL of double-distilled water in a round-bottom flask and stirred at 40°C until complete dissolution and was added slowly into clay suspension. The mixture was stirred for 24 h on magnetic stirrer followed by sonication using ultrasound equipment for 30 min. The final solution was degassed under vacuum for 30 min in order to remove all bubbles. Now the above prepared homogeneous solution was poured into polystyrene glass Petri dish and placed in a hot air oven for complete evaporation of solvent at 60°C. The dried sample was crushed in fine particles and stored for characterization and adsorption studies.

### 2.4. Adsorbent characterization

The FTIR spectra of the adsorbent materials were recorded with a Perkin-Elmer 1800 model IR spectrophotometer operating in a frequency range from

400 to 4,000  $\text{cm}^{-1}$  using KBr pellets, XRD patterns of the samples were examined using Siemens D 5005 X-ray unit Cu  $K\alpha$  ( $\lambda = 1.5406 \text{ \AA}$ ) radiation, generated at a voltage of 40 kV, and a current of 40 mA was used as the X-ray source. Scanning electron microscopy and electron diffraction scattering analysis were done using JEOL GSM 6510LV scanning electron microscope. The particle size and structure of the synthesized nanocomposite were observed using JEOL JEM 2100 TEM. Differential scanning calorimetry (DSC) thermograms were recorded with a Perkin–Elmer Pyris 6 under  $\text{N}_2$  atmosphere at a heating rate of  $10^\circ\text{C min}^{-1}$  to measure glass transition temperature ( $T_g$ ). Thermogravimetric analysis was performed with DuPont Instruments (TGA 951) analyser at  $10^\circ\text{C min}^{-1}$  heating rate under nitrogen atmosphere in the temperature range of 30–800°C to determine dynamic weight loss. The concentration of metal ions in the solution was measured using atomic absorption spectrophotometer GBC 902. Elico Li 120 pH meter was used to adjust the pH of the solutions.

### 2.5. Adsorption experiments

Adsorption experiments were carried out using batch techniques. A known amount (0.05 g) of adsorbent was thoroughly mixed at 120 rpm with 20 mL of respective metal ion solutions, with known concentration and pH values in a shaker. The pH of the reaction mixture was initially adjusted using either hydrochloric acid (0.1 M) or sodium hydroxide (0.1 M). At the end of desired exposure time, the suspensions were filtered using whatman filter paper (0.45 mm) and the filtrates were analysed by AAS.

Experimental variables considered were initial concentration of metal ions (10–100  $\text{mg L}^{-1}$ ), pH (2–7), dosage of nanocomposite (0.01–0.1 g) and contact time (5–240 min). For optimization of the adsorption, one parameter was varied at a time keeping the others fixed. Adsorption isotherm studies were carried out with five different initial concentrations (20–100  $\text{mg L}^{-1}$ ) of heavy metal ions. Langmuir, Freundlich, Tempkin and D–R models were applied to the adsorption isotherm, and different constants were generated. Kinetic and thermodynamic studies were also conducted in order to evaluate the nature of adsorption process.

If  $q_e$  is the amount of metal adsorbed per specific amount of adsorbent ( $\text{mg g}^{-1}$ ), the adsorption capacity at the time  $t$ ,  $q_t$  ( $\text{mg g}^{-1}$ ) is obtained using the Eq. (1):

$$q_e = \frac{(C_o - C_e)V}{W} \quad (1)$$

where  $C_o$  and  $C_e$  ( $\text{mg L}^{-1}$ ) are the initial and equilibrium concentrations of metal ions,  $V$  (L) is the volume of metal ion taken, and  $W$  is the mass of adsorbent in gram.

## 3. Results and discussion

### 3.1. Characterization of Alg-Cys-MMT nanocomposite

FTIR provides specific information about chemical bonding and molecular structures. In this study, FTIR analysis was applied to examine the possible interactions between the components of the nanocomposite. The FTIR spectra of MMT, Cys-MMT, Alg and Alg-Cys-MMT are shown in Fig. 1. FTIR spectrum of Na-MMT showed the band at  $474 \text{ cm}^{-1}$  (Si–O–Si deformation),  $534 \text{ cm}^{-1}$  (Si–O–Al deformation),  $1,046 \text{ cm}^{-1}$  (Si–O stretching),  $1,646 \text{ cm}^{-1}$  (O–H deformation),  $3,408$  and  $3,640 \text{ cm}^{-1}$  (O–H stretching) [18]. In the FTIR spectrum of Cys-MMT, in relation to the covalent binding between MMT and cysteine, all the peaks are characteristics of MMT with little bit of shift except the peaks at  $1,489 \text{ cm}^{-1}$  are N–H bendings and the band at  $1,409 \text{ cm}^{-1}$  is a C=N stretching band. The C=O carbonyl band was seen at  $1,629 \text{ cm}^{-1}$ . O–H bending band of MMT was split and it was clearly seen in the spectrum. From these results, it seems that MMT interacts with the  $-\text{NH}_2$  groups of cysteine. FTIR spectrum of alginate exhibited absorption bands at  $3,450 \text{ cm}^{-1}$  (OH stretching),  $2,920 \text{ cm}^{-1}$  ( $\text{CH}_2$  stretching),  $1,622 \text{ cm}^{-1}$  (COO $^-$  asymmetric stretching) and  $1,426 \text{ cm}^{-1}$  (COO $^-$  symmetric stretching). The bands at  $852$ – $1,160 \text{ cm}^{-1}$  are due to the O–C–O stretching of ether groups and the C–O stretching of alcoholic groups [19]. In the FTIR spectrum of Alg-Cys-MMT, incorporation of nanoclay in alginate matrix increased the intensity of  $\text{CH}_2$  stretching peaks and the absorption wavelength of the COO peaks shifts to  $3,402 \text{ cm}^{-1}$  with the loading of MMT clay to alginate. There is a new peak at  $2,110 \text{ cm}^{-1}$  which corresponds to  $\text{NH}_3^+$  stretching vibration.

XRD is a versatile and non-destructive technique that is used for the identification of the crystalline phases and the structural properties of the materials. XRD patterns of MMT, Cys-MMT, Alg and Alg-Cys-MMT nanocomposite are shown in Fig. 2. The diffraction peak of the Cys-MMT occurring at  $2\theta = 26.69^\circ$ , corresponding to  $3.336 \text{ \AA}$ , shifted from that of Na-MMT ( $2\theta = 28.94^\circ$ ), corresponding to  $3.01 \text{ \AA}$ . These indicated that the cation exchange is intercalated into the galleries of silicate layers after exchanging with the sodium ion. Thus, MMT is successfully modified by the amino acid. After intercalation with alginate, the characteristic peak related to clay is not disappeared and still present in

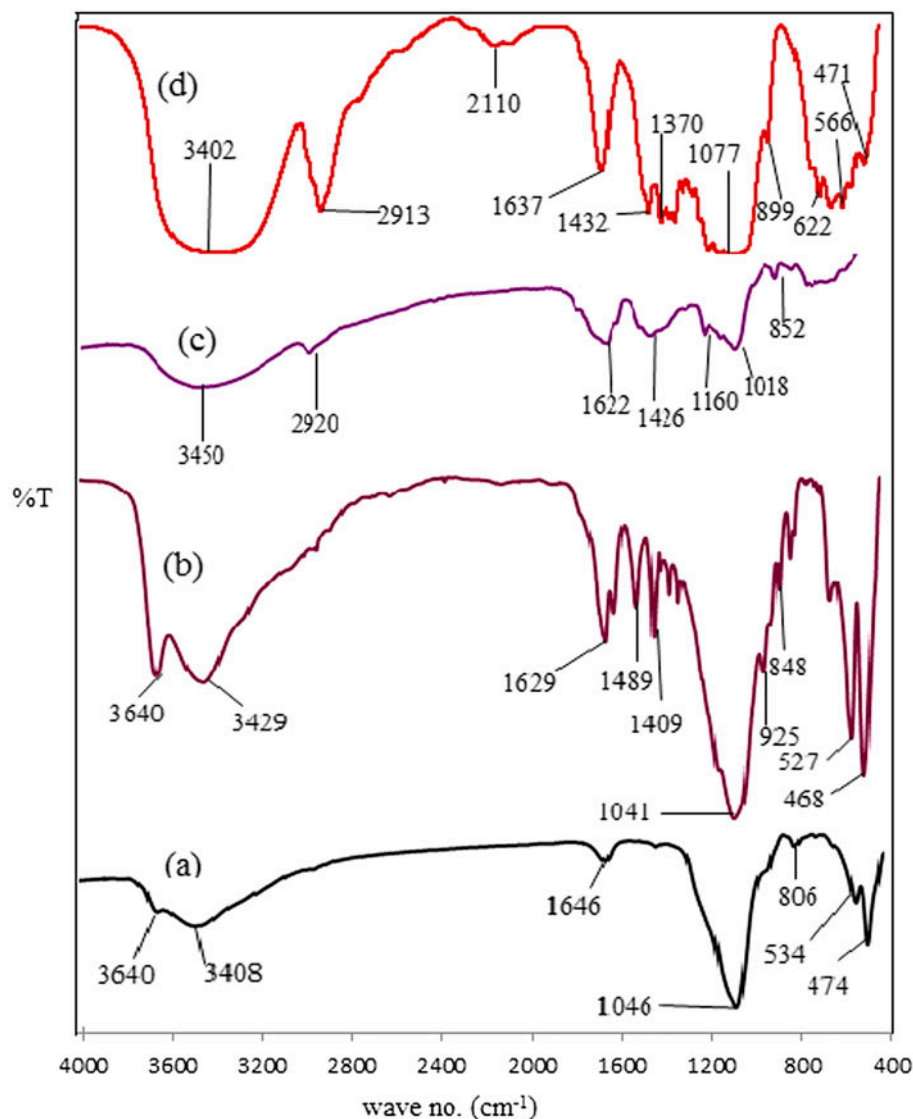


Fig. 1. FTIR spectra of (a) MMT (b) Cys-MMT (c) alginate and (d) Alg-Cys-MMT.

position  $2\theta = 26.72^\circ$ . Accordingly, it is suggested that the Cys-MMT nanoclay are intercalated in alginate matrix.

The morphologies of alginate and Alg-Cys-MMT nanocomposite were investigated by SEM. The SEM images of the samples are shown in Fig. 3 with their EDX graphs. The SEM micrograph for alginate revealed irregular spherical granules. After intercalation of alginate into the MMT layers, the granular structure of alginate had changed to a fracture surface and the Alg-Cys-MMT nanocomposites displayed an oriented fracture probably due to the orientation of the nanoclay into the alginate matrix.

Thermogravimetric analysis (TGA) of alginate and the prepared nanocomposites were measured under a

nitrogen atmosphere in the temperature range 30–800°C in order to investigate the thermal stability. TGA graph given in Fig. 4 indicates that the prepared bio-nanocomposite decomposes at a higher temperature in three stages with good thermal properties (residual weight per cent 40%) as compared to neat alginate which undergoes decomposition at relatively low temperature (residual weight per cent 15%). It indicates that the incorporation of 5% w/w Cys-MMT in alginate matrix exhibited an enhanced thermal stability. This improvement in thermal stability may attribute to the inherently good thermal properties of inorganic clays that prevent the quick transmission of heat and limit any further decomposition of the nanocomposites [20,21].

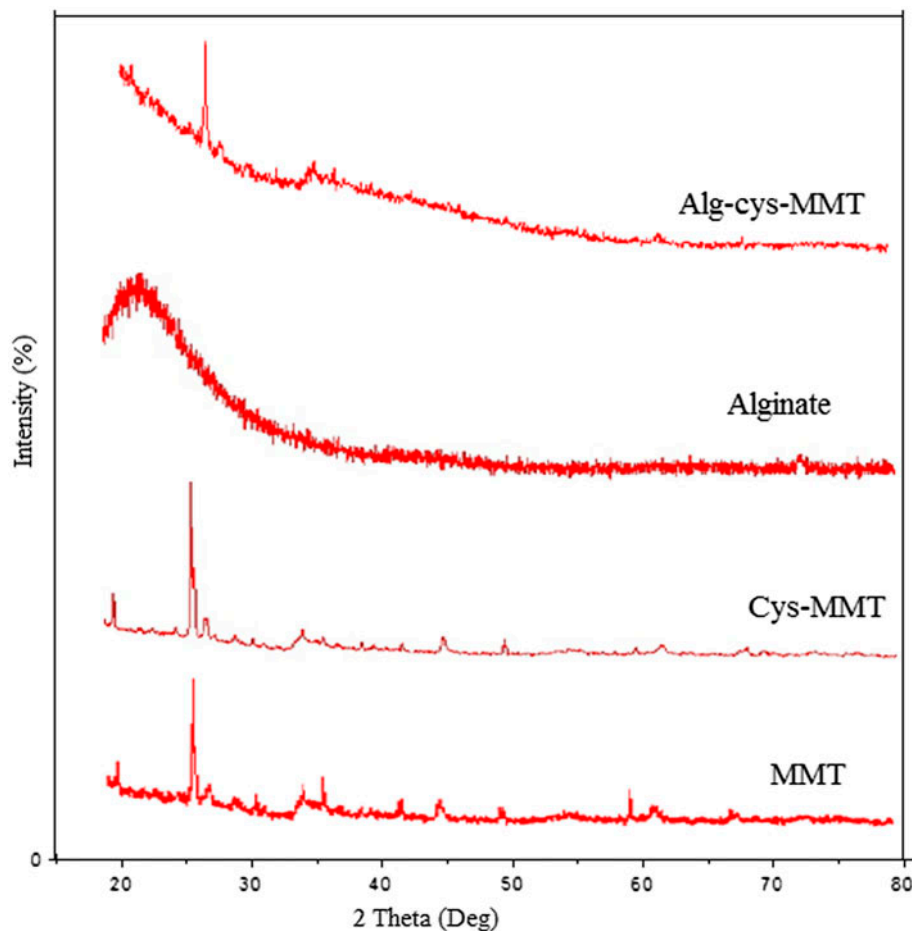


Fig. 2. XRD spectra of individuals and nanocomposite material.

DSC can be used to measure glass transition temperatures  $T_g$  of the polymers. From the Fig. 5, the glass transition temperature ( $T_g$ ) of pure alginate and its nanocomposite is found to be 50 and 53°C, respectively. As the temperature increases, an amorphous biopolymer and its nanocomposite will become less viscous. At some point, the molecules may obtain enough freedom of motion to spontaneously arrange themselves into a crystalline form and the exothermic peak in the Fig. 5 is due to the crystallization of molecules in the material which occurs at 90.12°C for alginate and 77.95°C for nanocomposite material. As the temperature increases, the sample eventually reaches its melting temperature ( $T_m$ ). The melting process results in an endothermic peak in the DSC curve. As can be seen, the melting temperature of Alg-Cys-MMT nanocomposite is higher (289.77°C) than the pure alginate biopolymer (271.46°C) due to intercalation of MMT in the biopolymer matrix.

More information about the microstructures of Alg-Cys-MMT nanocomposites containing 5.0 wt.% nanoclay was obtained by TEM observations. The suspended phase of Alg-Cys-MMT nanocomposites was shown in Fig. 6. Many dark, distinct spherical particles (70 nm) were distributed in the micrograph. Surprisingly, the nanoclay particles in the nanocomposite are randomly distributed.

### 3.2. Effect of contact time and initial metal ion concentration

The effect of contact time on adsorption of metal ions ( $\text{Cu}^{2+}$ ,  $\text{Pb}^{2+}$  and  $\text{Ni}^{2+}$ ) onto Alg-Cys-MMT nanocomposite was studied in the range of 5–240 min using 50 mg L<sup>-1</sup> as initial metal ion concentration at 50°C. Fig. 7 shows that the amount of heavy metal ions adsorbed per unit mass of adsorbent increased

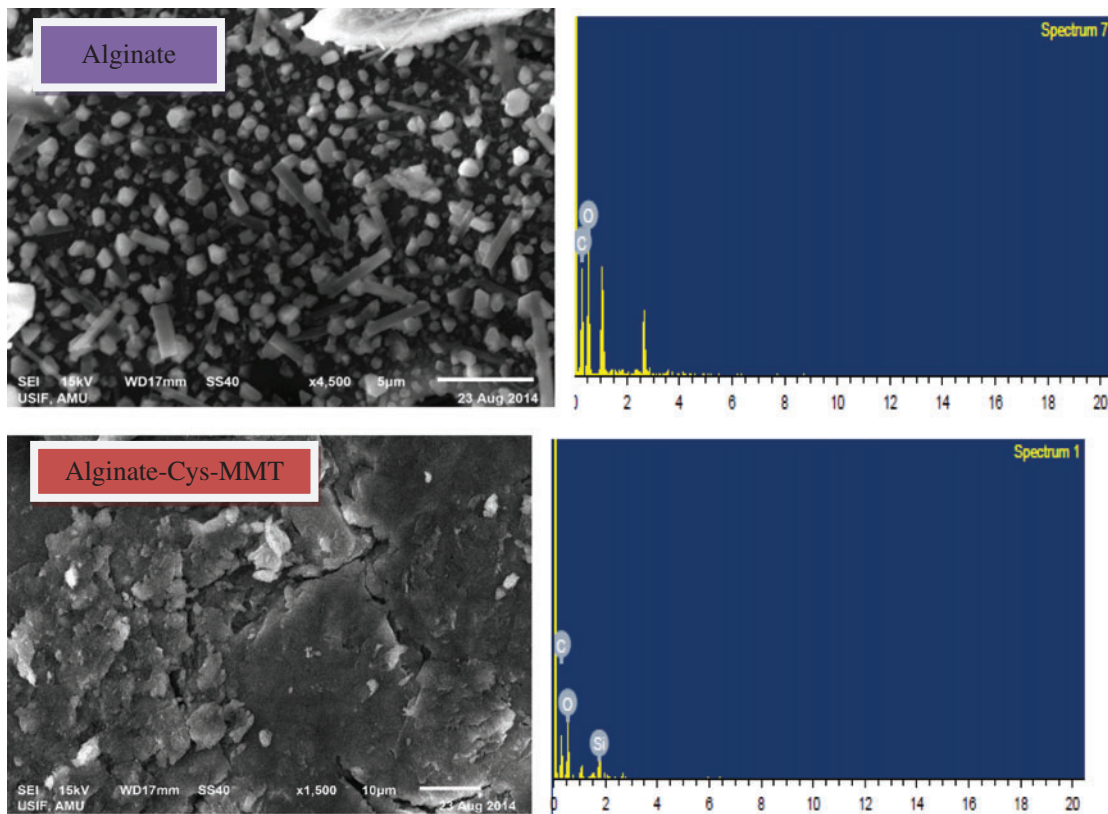


Fig. 3. SEM images of alginate and Alg-Cys-MMT with their EDS images.

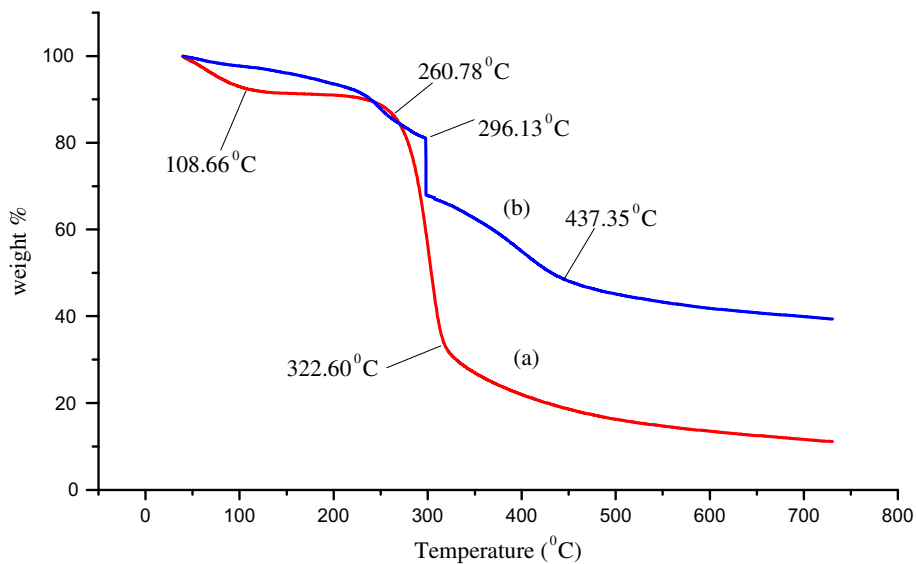


Fig. 4. TGA thermograms of (a) alginate and (b) Alg-Cys-MMT.

rapidly within 30 min and slowly reaches the saturation at about 120 min. The initial rapid phase is probably due to the abundant availability of reaction

sites, and with gradual utilization of these sites, the adsorption becomes less efficient in the lower stage. We did not find any significant influence of contact

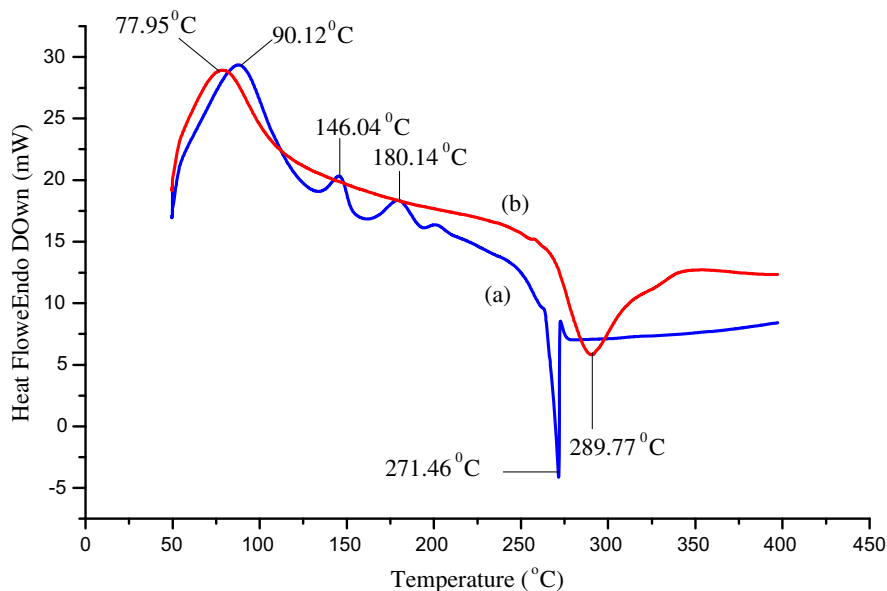


Fig. 5. DSC thermograms of (a) alginate and (b) Alg-Cys-MMT.

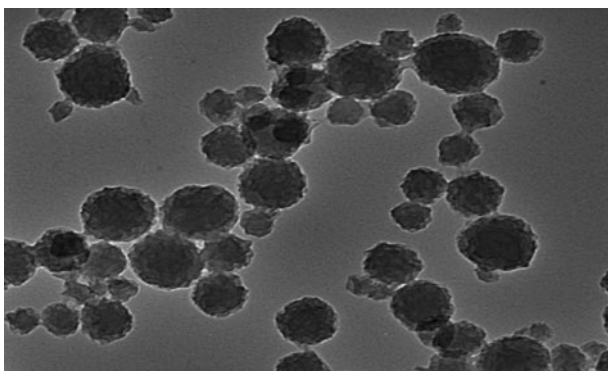


Fig. 6. TEM image of Alg-Cys-MMT nanocomposite showing the distribution of nanoclay in the alginate matrix.

time on the adsorption efficiency after contact time of 120 min. The time profile of heavy metal ions uptake is a single, smooth and continuous curve leading to saturation, suggesting the affinity of heavy metals on the surface of the adsorbent. The equilibrium time of 120 min can be considered very short, which is an economically favourable condition for the adsorbent described here. Based on these results, a contact time of 120 min was selected for all subsequent batch experiments.

The experimental values of adsorption capacity of Alg-Cys-MMT nanocomposite for metal ions at the equilibrium were 17.60, 18.76 and 19.96 ( $\text{mg g}^{-1}$ ) for  $\text{Cu}^{2+}$ ,  $\text{Pb}^{2+}$  and  $\text{Ni}^{2+}$  ions, respectively, as shown in Fig. 7. The data indicate that the initial metal ion

concentration determines the equilibrium concentration and also determines the uptake rate of metal ions and the kinetic character of metal uptake [22]. The rate parameters were depicted in the Table 2. Adsorption capacity ( $\text{mg g}^{-1}$ ) increased from 5.16 to 23.54 for  $\text{Cu}^{2+}$ , 8.16 to 26.04 for  $\text{Pb}^{2+}$  and 13.59 to 41.05 for  $\text{Ni}^{2+}$  as initial concentration increased from 20 to 100  $\text{mg L}^{-1}$ . This might be due to the fact that increasing metal ion concentration increased the number of collision between the adsorbent and metal ion species, this leading an increased metal uploading on adsorbent surface [23]. We have kept initial metal ion concentration constant as 50  $\text{mg L}^{-1}$  for all optimization process.

### 3.3. Effect of pH

The initial pH value of the solution is an important factor that must be considered during adsorption studies. Experiments were performed in the pH range of 2.0–7.0 for an initial metal ion concentration of 50  $\text{mg L}^{-1}$  at 25°C for 120 min, where chemical precipitation is avoided, so that the removal could be related to the adsorption process. After filtration, the metal ion concentrations in the supernatants were determined by AAS. Fig. 8 shows the effect of pH on the adsorption of metal ions onto synthesized (Alg-Cys-MMT) nanocomposite. At low pH due to high  $\text{H}^+$  concentration, active sites on the adsorbent get protonated resulting in a low removal efficiency of heavy metals.

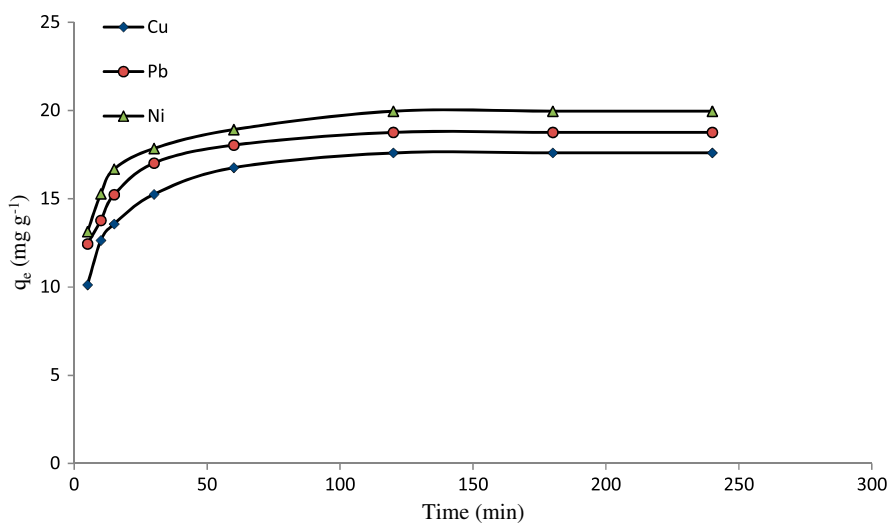


Fig. 7. Effect of time for the adsorption of  $\text{Cu}^{2+}$ ,  $\text{Pb}^{2+}$  and  $\text{Ni}^{2+}$  onto Alg-Cys-MMT nanocomposite at  $50 \text{ mg L}^{-1}$  as initial metal ion concentration at  $25^\circ\text{C}$ .

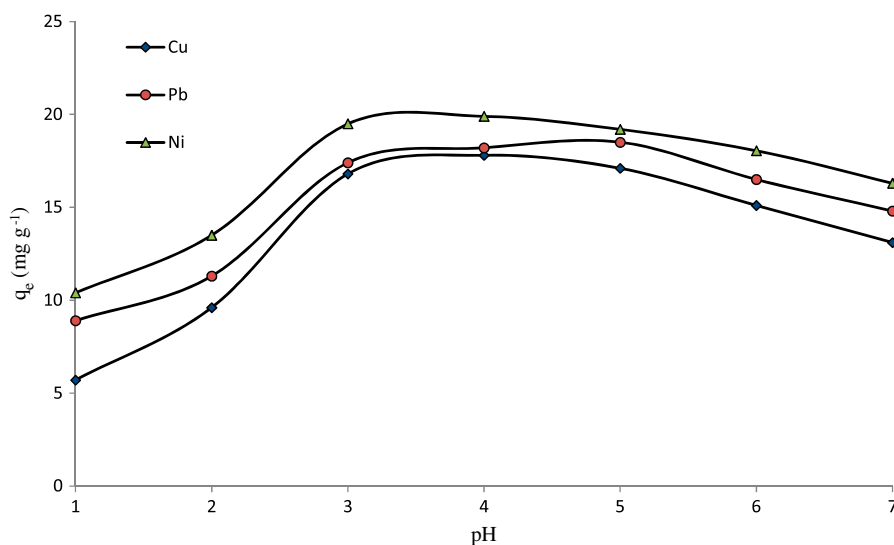


Fig. 8. Effect of pH for the adsorption of  $\text{Cu}^{2+}$ ,  $\text{Pb}^{2+}$  and  $\text{Ni}^{2+}$  onto Alg-Cys-MMT nanocomposite with initial concentration of each metal ion ( $C_0 = 50 \text{ mg L}^{-1}$ ) at  $25^\circ\text{C}$ .

As the pH of the solution increases, the removal efficiency also increases, reaching plateau values around pH 4 for  $\text{Cu}^{2+}$ , 5 for  $\text{Pb}^{2+}$  and 4 for  $\text{Ni}^{2+}$ . At optimum pH, the experimental adsorption capacities ( $\text{mg g}^{-1}$ ) for  $\text{Cu}^{2+}$ ,  $\text{Pb}^{2+}$  and  $\text{Ni}^{2+}$  ions are found to be 17.8, 18.5 and 19.9, respectively. The decrease in the adsorption of  $\text{Cu}^{2+}$ ,  $\text{Pb}^{2+}$  and  $\text{Ni}^{2+}$  ions at a pH more than the optimum pH was due to the formation of hydroxylated complexes of these metal ions in the solutions [24].

### 3.4. Effect of adsorbent dose

The effect of the adsorbent dosage on the adsorption of  $\text{Cu}^{2+}$ ,  $\text{Pb}^{2+}$  and  $\text{Ni}^{2+}$  was investigated in the range of 0.01–0.1 g in 20 mL of metal ions solutions with the initial metal ion concentration of  $50 \text{ mg L}^{-1}$ ,  $50^\circ\text{C}$  and optimum pH. As can be seen in Fig. 9, the  $\text{Cu}^{2+}$ ,  $\text{Pb}^{2+}$  and  $\text{Ni}^{2+}$  ions removal efficiency by adsorbent was maximum at 0.05, 0.07 and 0.08 g and then declined. By increasing the concentration of the

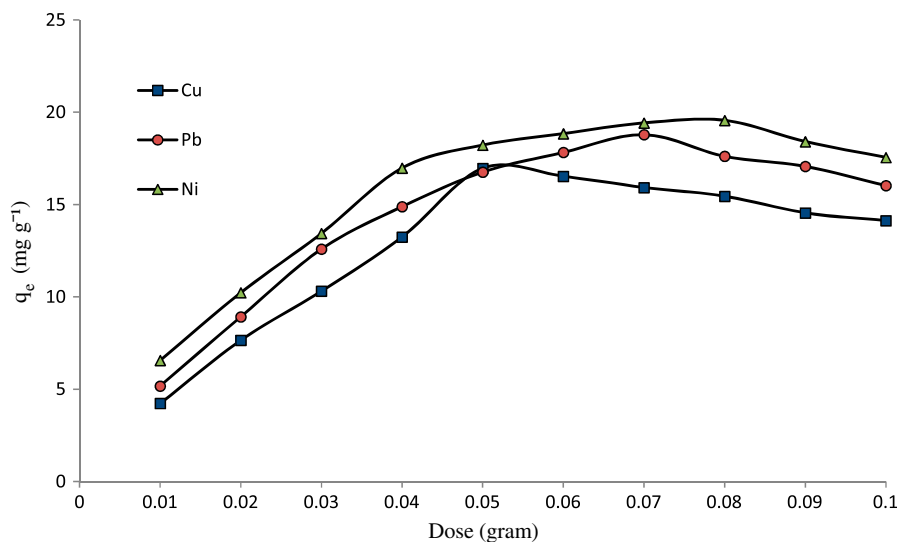


Fig. 9. Effect of adsorbent dosage for the adsorption of  $\text{Cu}^{2+}$ ,  $\text{Pb}^{2+}$  and  $\text{Ni}^{2+}$  onto Alg-Cys-MMT nanocomposite with initial concentration of each metal ion ( $C_0 = 50 \text{ mg L}^{-1}$ ) at  $25^\circ\text{C}$ .

adsorbent, access to the residual sites for metal ions adsorption was restricted. In addition, the effective surface area for adsorption decreased due to the partial aggregation of the adsorbent at high adsorbent concentrations leading to a decrease in the adsorption capacity of the metal ions. Consequently, for further experiments, 0.05 g was selected for all metals as optimum dose.

### 3.5. Adsorption isotherm models

Adsorption isotherms are of great importance in the design of adsorption systems because they can reflect the surface and adsorption characteristics of adsorption capacity, adsorption strength and adsorption state of adsorbent. Adsorption equilibrium data were applied to Langmuir, Freundlich, D-R and Tempkin isotherms at  $50^\circ\text{C}$ , and the linear fitting results were shown in Table 1.

#### 3.5.1. Langmuir adsorption isotherm

The theoretical Langmuir isotherm model is often used to describe the equilibrium adsorption isotherms of homogeneous surfaces. This isotherm model assumes that all sites possess equal affinity for the adsorbate. In this theory, the adsorption reaches to its maximum level after a complete monolayer formation of adsorbate molecules onto the adsorbent surface [25]. Mathematically, the equation can be written as follows:

$$\frac{C_e}{q_e} = \frac{1}{q_m K_L} + \frac{C_e}{q_m} \quad (2)$$

where  $q_m$  is the maximum metal ion uptake capacity ( $\text{mg g}^{-1}$ ),  $K_L$  is the Langmuir constant related to the adsorption energy ( $\text{L mg}^{-1}$ ), and  $q_e$  and  $C_e$  are defined as adsorption capacity ( $\text{mg g}^{-1}$ ) and equilibrium concentration ( $\text{mg L}^{-1}$ ). Using the linear Langmuir isotherm equation, the isotherm constants were calculated from the plot between  $C_e/q_e$  and  $C_e$  (Fig. 10) and the results are tabulated in Table 1. From this research work, the maximum monolayer coverage capacity  $q_m$  ( $\text{mg g}^{-1}$ ) for  $\text{Cu}^{2+}$ ,  $\text{Pb}^{2+}$  and  $\text{Ni}^{2+}$  ions from Langmuir isotherm model was determined to be 125.0, 111.11 and 100.0 for  $K_L$  (Langmuir isotherm constant) values of 0.076, 0.117 and 0.185  $\text{L mg}^{-1}$  and the  $R^2$  value is 0.99 proving that the sorption data fitted well to Langmuir isotherm model.

#### 3.5.2. Freundlich adsorption isotherm

The Freundlich isotherm model is the earliest empirical equation based on the adsorption on reversible heterogeneous surfaces. The mathematical expression of the model is given as follows [26]:

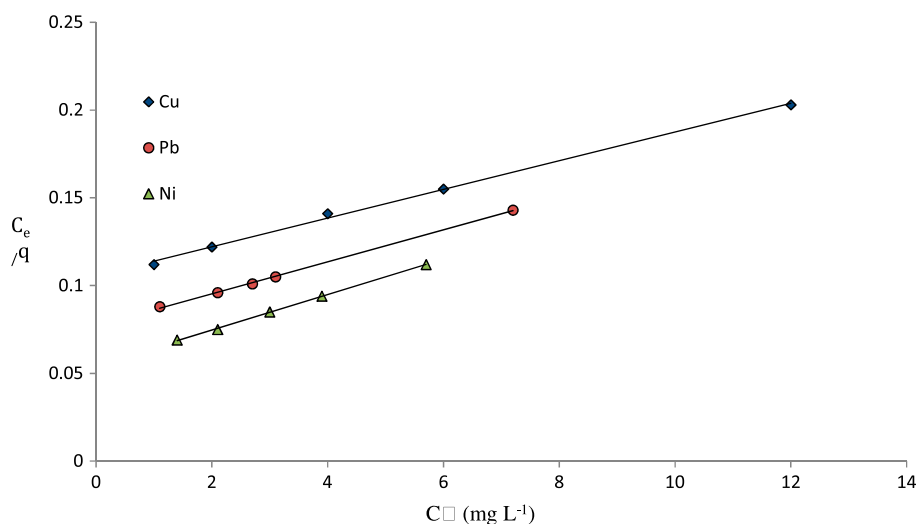
$$\ln q_e = \frac{1}{n} \ln C_e + \ln K_F \quad (3)$$

where  $1/n$  is a numerical value related to the adsorption intensity which varies with the heterogeneity, and  $K_F$  indicates the adsorption capacity. The value of  $n$

Table 1

Adsorption isotherm parameters for the adsorption of  $\text{Cu}^{2+}$ ,  $\text{Pb}^{2+}$  and  $\text{Ni}^{2+}$  onto Alg-Cys-MMT nanocomposite at  $50^\circ\text{C}$ 

Isotherm models	Parameters	Metals		
		$\text{Cu}^{2+}$	$\text{Pb}^{2+}$	$\text{Ni}^{2+}$
Langmuir	$q_m$ ( $\text{mg g}^{-1}$ )	125.0	111.11	100.0
	$K_L$ ( $\text{L mg}^{-1}$ )	0.076	0.117	0.185
	$R^2$	0.999	0.999	0.999
Freundlich	$K_F$ ( $\text{mg g}^{-1}$ )	5.328	7.53	12.23
	$n$	1.56	1.43	1.56
	$R^2$	0.979	0.998	0.985
Tempkin	$A$ ( $\text{L gm}^{-1}$ )	1.713	1.726	1.754
	$B$ ( $\text{J mol}^{-1}$ )	7.725	10.53	16.02
	$R^2$	0.980	0.964	0.992
Dubinin–Radushkevich (D–R)	$q_m$ ( $\text{mg g}^{-1}$ )	21.26	26.26	42.37
	$k_{D-R}$ ( $\text{mol}^2 \text{kJ}^{-2}$ )	$5 \times 10^7$	$4 \times 10^7$	$5 \times 10^7$
	$E$ ( $\text{kJ mol}^{-1}$ )	10.47	11.70	10.47
	$R^2$	0.980	0.970	0.986

Fig. 10. Langmuir isotherm for the adsorption of  $\text{Cu}^{2+}$ ,  $\text{Pb}^{2+}$  and  $\text{Ni}^{2+}$  onto Alg-Cys-MMT nanocomposite at  $50^\circ\text{C}$  and optimum pH for each metal ion.

and  $K_F$  can be calculated by a linear plot between  $\ln q_e$  and  $\ln C_e$  (Fig. 11), and the data obtained are given in Table 1. As perceived in Table 1, the  $n$  value is more than the unit indicating a favourable adsorption of  $\text{Cu}^{2+}$ ,  $\text{Pb}^{2+}$  and  $\text{Ni}^{2+}$  on the surface of the adsorbent. From the data in Table 1, that value of  $n$  for  $\text{Cu}^{2+}$ ,  $\text{Pb}^{2+}$  and  $\text{Ni}^{2+}$  ions is 1.56, 1.43 and 1.56 indicating that the sorption of metal ions onto Alg-Cys-MMT is favourable and the  $R^2$  value is 0.97, 0.99 and 0.98.

### 3.5.3. Dubinin–Radushkevich adsorption isotherm

D–R isotherm is generally applied to express the adsorption mechanism with a Gaussian energy distribution onto a heterogeneous surface [27]. The model has often successfully fitted high solute activities and the intermediate range of concentrations.

$$\ln q_e = \ln q_m - k_{D-R} \varepsilon^2 \quad (4)$$

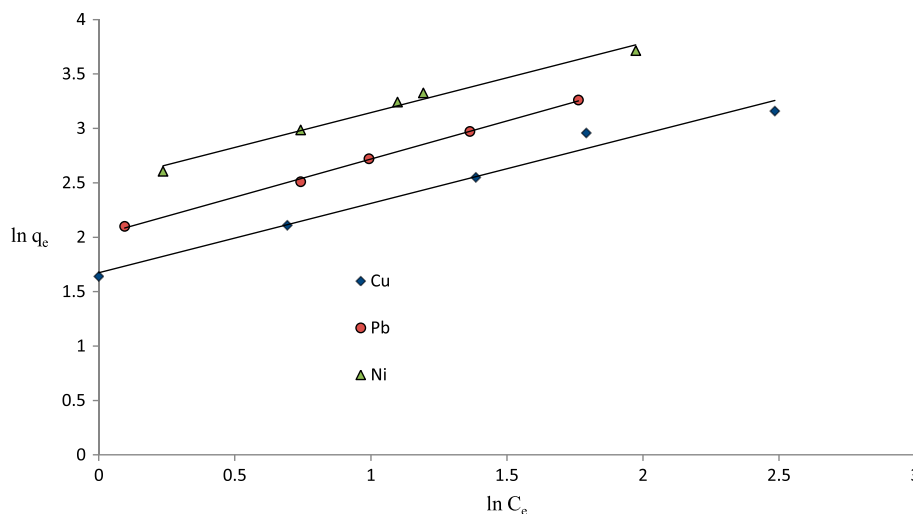


Fig. 11. Freundlich isotherms for the adsorption of  $\text{Cu}^{2+}$ ,  $\text{Pb}^{2+}$  and  $\text{Ni}^{2+}$  onto Alg-Cys-MMT nanocomposite at  $50^\circ\text{C}$  and optimum pH for each metal ion.

where  $q_e$  is the amount of adsorbate in the adsorbent at equilibrium ( $\text{mg g}^{-1}$ );  $q_m$  is the theoretical isotherm saturation capacity ( $\text{mg g}^{-1}$ );  $K_{\text{ad}}$  is Dubinin–Radushkevich isotherm constant ( $\text{mol}^2 \text{kJ}^{-2}$ ); and  $\varepsilon$  is Dubinin–Radushkevich isotherm constant. The approach was usually applied to distinguish the physical and chemical adsorption of metal ions with its mean free energy. The  $E$  per molecule of adsorbate (for removing a molecule from its location in the sorption space to the infinity) can be computed by the relationship.

$$E = \frac{1}{\sqrt{2k_{\text{D-R}}}} \quad (5)$$

$\varepsilon$  is Polanyi potential which is related to the equilibrium concentration as follows:

$$\varepsilon = RT \ln \left( 1 + \frac{1}{C_e} \right) \quad (6)$$

where  $R$ ,  $T$  and  $C_e$  represent the gas constant ( $8.314 \text{ J mol}^{-1} \text{ K}^{-1}$ ), absolute temperature (K) and adsorbate equilibrium concentration ( $\text{mg L}^{-1}$ ), respectively. One of the unique features of the D–R isotherm model lies on the fact that it is temperature-dependent and when adsorption data at different temperatures are plotted as a function of logarithm of amount adsorbed  $\ln q_e$  vs. the square of potential energy, all suitable data will lie on the same curve, named as the characteristic curve Fig. 12 [28]. The constants such as  $q_m$  and  $K_{\text{ad}}$  were determined from the appropriate plot using Eq. (4) above. From the linear plot of D–R

model,  $q_m$  ( $\text{mg g}^{-1}$ ) was determined to be 21.61 for  $\text{Cu}^{2+}$ , 26.26 for  $\text{Pb}^{2+}$  and 42.37 for  $\text{Ni}^{2+}$ , the mean free energy,  $E$  ( $\text{kJ/mol}$ ), is 10.47 for  $\text{Cu}^{2+}$ , 11.70 for  $\text{Pb}^{2+}$  and 10.47 for  $\text{Ni}^{2+}$  indicating a chemisorption process.

#### 3.5.4. Tempkin isotherm model

This isotherm contains a factor that explicitly takes into account of adsorbent–adsorbate interactions. The Tempkin isotherm model is based on two assumptions: (i) heat of adsorption would decrease linearly rather than logarithmic with the coverage and (ii) its derivation is characterized by a uniform distribution of binding energies up to some maximum binding energy [29]. The Tempkin isotherm equation would be:

$$q_e = B \ln A + B \ln C_e \quad (7)$$

where  $B = RT/b$  and  $A$  ( $\text{L mg}^{-1}$ ) is Tempkin constant representing the equilibrium binding. The mentioned isotherm constants were calculated from the plot between  $q_e$  and  $\ln C_e$  from Fig. 13, and the results are listed in Table 1. As can be seen from the Table 1, the binding constant is maximum for  $\text{Ni}^{2+}$  followed by  $\text{Pb}^{2+}$  and then  $\text{Cu}^{2+}$  supporting the maximum affinity shown by  $\text{Ni}^{2+} > \text{Pb}^{2+} > \text{Cu}^{2+}$ .

#### 3.6. Adsorption kinetics

The adsorption kinetics process was investigated by four kinetic models: Lagergren pseudo-first-order, pseudo-second-order, Elovich equation and intraparticle

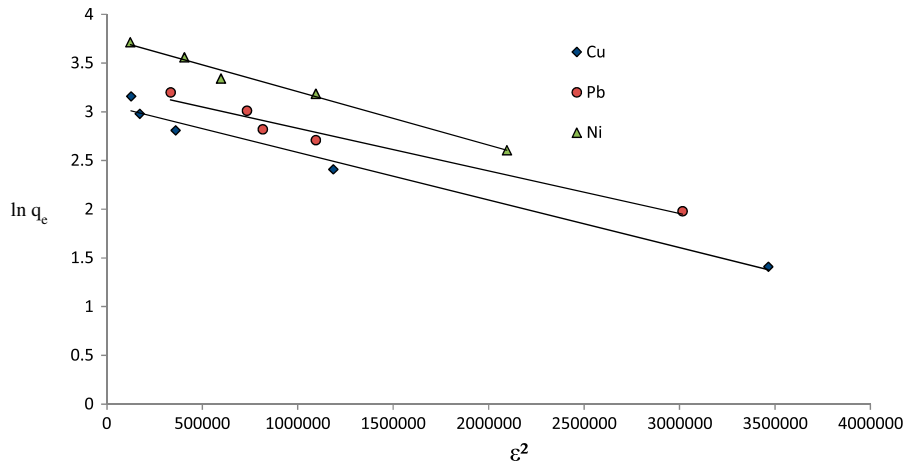


Fig. 12. D-R isotherm for the adsorption of  $\text{Cu}^{2+}$ ,  $\text{Pb}^{2+}$  and  $\text{Ni}^{2+}$  onto Alg-Cys-MMT nanocomposite at  $50^\circ\text{C}$  and optimum pH for each metal ion.

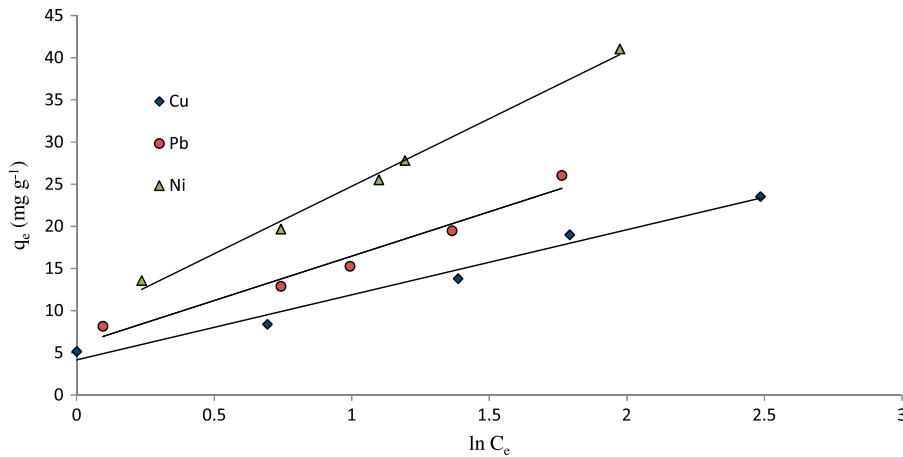


Fig. 13. Tempkin isotherm for the adsorption of  $\text{Cu}^{2+}$ ,  $\text{Pb}^{2+}$  and  $\text{Ni}^{2+}$  onto Alg-Cys-MMT nanocomposite at  $50^\circ\text{C}$  and optimum pH for each metal ion.

diffusion. Parameters of the kinetic models and coefficients of determination ( $R^2$ ) were calculated to determine the conformity of the models with the experimental data; the results are presented in Table 2. Figs. 14–18 shows the linear plots of the kinetic models for all the tested metal ions.

### 3.6.1. Lagargren pseudo-first-order

A kinetic model for the adsorption analysis that is preceded by diffusion through a boundary will most likely follow the pseudo-first-order equation of Lagargren [30]:

$$\log(q_e - q_t) = \log q_e - \frac{k_1}{2.303} t \tag{8}$$

where  $q_e$  and  $q_t$  represent the amount of heavy metal ions absorbed on the adsorbent ( $\text{mg g}^{-1}$ ) at equilibrium and time  $t$ , respectively.  $K_1$  is the rate constant of the pseudo-first-order kinetics. The value of adsorption rate constant  $K_1$  and  $q_e$  is calculated from the straight line plot of  $\log(q_e - q_t)$  vs. time shown in Fig. 14.

### 3.6.2. Pseudo-second-order

The pseudo-second-order kinetic model notes that the adsorption should relate to the squared product of the difference between the number of the equilibrium adsorptive sites available on an adsorbent and that of the occupied sites. This model is expressed as follows [31,32]:

Table 2

Kinetic parameters for the adsorption of  $\text{Cu}^{2+}$ ,  $\text{Pb}^{2+}$  and  $\text{Ni}^{2+}$  onto Alg-Cys-MMT nanocomposite at 50 ppm as initial metal ion concentration

Kinetic models	Parameters	Metals		
		$\text{Cu}^{2+}$	$\text{Pb}^{2+}$	$\text{Ni}^{2+}$
Pseudo-first-order	$q_e$ ( $\text{mg g}^{-1}$ )	7.320	6.560	5.880
	$K_1$ ( $\text{min}^{-1}$ )	0.032	0.034	0.034
	$R^2$	0.984	0.984	0.987
Pseudo-second-order	$q_e$ ( $\text{mg g}^{-1}$ ) (cal)	18.18	19.2	20.41
	$K_2$ ( $\text{g mg}^{-1} \text{min}^{-1}$ )( $\times 10^{-3}$ )	0.012	0.015	0.015
	$q_e$ ( $\text{mg g}^{-1}$ ) (exp)	17.60	18.76	19.96
	$R^2$	0.999	0.999	0.999
Elovich	$\alpha$ ( $\text{mg g}^{-1} \text{min}^{-1}$ )	135.1	754.78	1,311.78
	$\beta$ ( $\text{g mg}^{-1}$ )	0.526	0.583	0.583
	$R^2$	0.934	0.928	0.952
Interparticle diffusion	$K_{\text{int}}$ ( $\text{mg g}^{-1} \text{min}^{-1/2}$ )	0.493	0.437	0.441
	$C$	11.29	13.18	14.25
	$R^2$	0.774	0.767	0.785

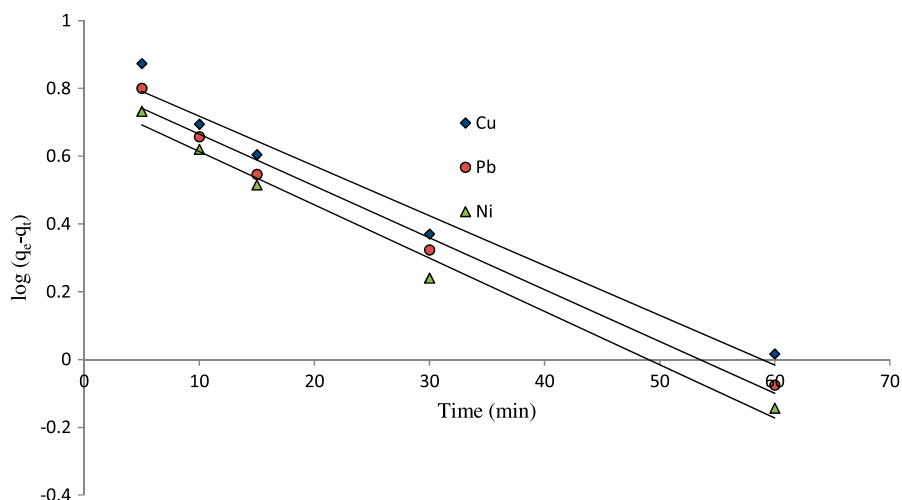


Fig. 14. Pseudo-first-order model for the adsorption of  $\text{Cu}^{2+}$ ,  $\text{Pb}^{2+}$  and  $\text{Ni}^{2+}$  onto Alg-Cys-MMT nanocomposite with initial concentration ( $C_0 = 50 \text{ mg L}^{-1}$ ) and optimum pH of each metal ion at  $25^\circ\text{C}$ .

$$\frac{t}{q_t} = \frac{1}{k_2 q_e^2} + \frac{t}{q_e} \quad (9)$$

where  $q_t$  ( $\text{mg g}^{-1}$ ) amount of metal ions adsorbed onto the surface of the nanocomposite at time  $t$ ,  $k_2$  is the pseudo-second-order rate constant ( $\text{g mg}^{-1} \text{min}^{-1}$ ), and  $q_e$  ( $\text{mg g}^{-1}$ ) is the amount of metal ion adsorbed at equilibrium. The pseudo-second-order constants can be calculated from the linear plot between  $t/q_t$  and time which is given in Fig. 15 and the calculated data are tabulated in Table 2. From the Table 2, the values of  $q_e$  calculated from the pseudo-second-order

kinetic models are very close to the experimental values in comparison with the values obtained from pseudo-first-order. The pseudo-second-order model has higher correlation coefficients ( $R^2 = 0.99$ ) than the pseudo-first-order model ( $R^2 = 0.98$ ) with experimental data. So pseudo-second-order kinetic model fits best to describe the sorption rate for all the tested metal ions.

### 3.6.3. Elovich model

The linear form of this equation is expressed as [33]:

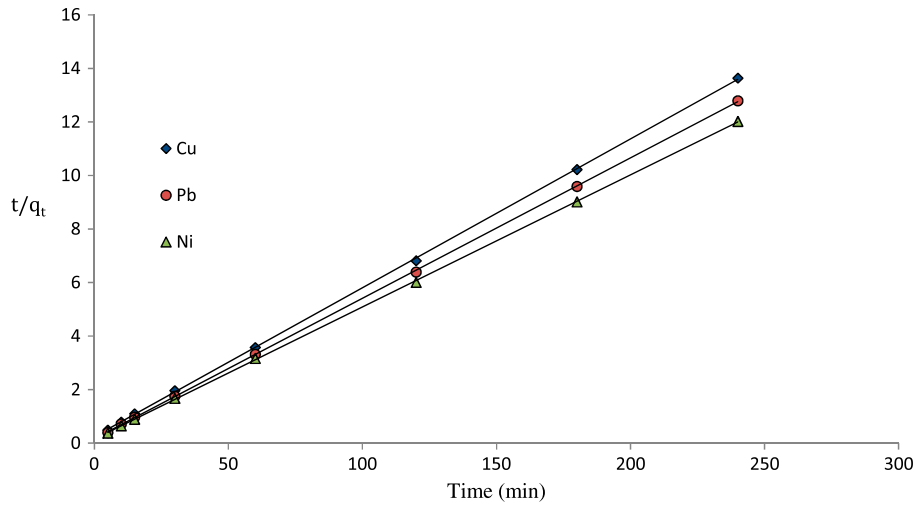


Fig. 15. Pseudo-second-order for the adsorption of  $\text{Cu}^{2+}$ ,  $\text{Pb}^{2+}$  and  $\text{Ni}^{2+}$  onto Alg-Cys-MMT nanocomposite with initial concentration ( $C_0 = 50 \text{ mg L}^{-1}$ ) and optimum pH of each metal ion at  $25^\circ\text{C}$ .

$$q_t = \frac{1}{\beta} \ln t + \frac{1}{\beta} \ln(\alpha\beta) \quad (10)$$

where  $\alpha$  is the initial adsorption rate ( $\text{mg g}^{-1} \text{ min}^{-1}$ ) and  $\beta$  is the adsorption constant ( $\text{g mg}^{-1}$ ) during any experiment. Fig. 16 shows a plot of linearization form of Elovich model. The slopes and intercepts of plots of  $q_t$  vs.  $\ln t$  were used to determine the constant  $\beta$  and the initial adsorption rate  $\alpha$ . However, the experimental data deviated considerably from the theoretical data. A comparison of the results with the correlation coefficients is shown in Table 2. The correlation

coefficients for the Elovich kinetic model obtained at all the studies concentrations were low as compared to pseudo-first-order and pseudo-second-order. This suggests that this adsorption system is not an acceptable for this system.

#### 3.6.4. Weber–Morris intraparticle diffusion model

This model can be expressed as:

$$q_t = K_{\text{int}} t^{0.5} + C \quad (11)$$

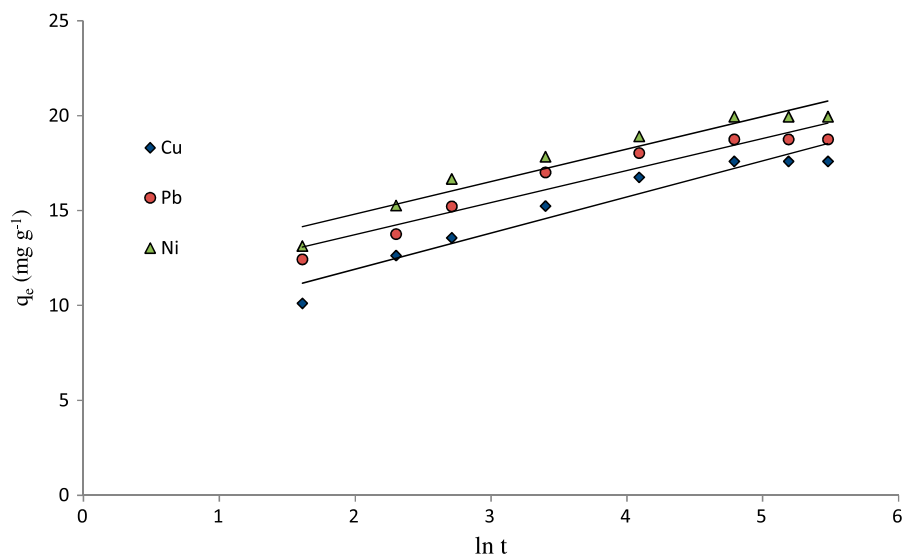


Fig. 16. Elovich model for the adsorption of  $\text{Cu}^{2+}$ ,  $\text{Pb}^{2+}$  and  $\text{Ni}^{2+}$  onto Alg-Cys-MMT nanocomposite with initial concentration ( $C_0 = 50 \text{ mg L}^{-1}$ ) and optimum pH of each metal ion at  $25^\circ\text{C}$ .

where  $K_{\text{int}}$  is the intraparticle diffusion rate constant ( $\text{mg g}^{-1} \text{min}^{1/2}$ ). The plot of  $q_t$  vs.  $t^{1/2}$  at different initial solution concentrations gives the value of  $K_{\text{int}}$  and may present multi-linearity which indicates two or more steps occurring in the adsorption process. The first sharper portion is the external surface adsorption or instantaneous adsorption stage. The second portion is the gradual adsorption stage where the intraparticle diffusion rate is controlled. The third is the final equilibrium stage where intraparticle diffusion starts to slow down due to extremely low solute concentration in the solution. The parameters calculated are given in Table 2. The intraparticle diffusion rate was obtained from the slope of the gentle-sloped portion (Fig. 17). From Table 2, with a low regression coefficient values for all metal ions, it seems this model is not fitting well for adsorption process.

### 3.7. Thermodynamic studies

When designing an adsorption system, the designer should put into consideration the change in the reaction and this change requires an idea of thermodynamics. Thermodynamics is based on the assumption that in an isolated system, where energy cannot be gained or lost to the surroundings, the entropy change is the driving force [34]. In environmental engineering practice, both energy and entropy factors must be considered in order to decide what processes will occur spontaneously. The thermodynamic parameters such as the Gibbs free energy change ( $\Delta G^\circ$ ), enthalpy change ( $\Delta H^\circ$ ) and entropy

change ( $\Delta S^\circ$ ) were determined using the following equations;

$$K_c = \frac{C_{\text{ad}}}{C_e} \quad (12)$$

$$\Delta G^\circ = -RT \ln K_c \quad (13)$$

$$\Delta G^\circ = \Delta H^\circ - T\Delta S^\circ \quad (14)$$

$$\ln K_c = -\frac{\Delta H^\circ}{R} + \frac{\Delta S^\circ}{RT} \quad (15)$$

The gas constant  $R$  is defined by  $8.3145 \text{ J mol}^{-1} \text{ K}^{-1}$ .  $K_c$  is the distribution coefficient;  $T$  is the temperature of the solution in Kelvin.  $\Delta H^\circ$  and  $\Delta S^\circ$ , the enthalpy and the entropy of adsorption for all metal ions, were calculated from the slope and intercept of a plot of  $\ln K_c$  as a function of  $1/T$  using Eq. (15) as shown in Fig. 18. The standard free energy ( $\Delta G^\circ$ ) can be calculated from Eq. (14).

Table 3 gives the values of the parameters for thermodynamic studies. The free energy change ( $\Delta G^\circ$ ) obtained during the adsorption reaction at temperatures of 30–50°C were all negative, and this indicates that the adsorption of  $\text{Cu}^{2+}$ ,  $\text{Pb}^{2+}$  and  $\text{Ni}^{2+}$  onto Alg-Cys-MMT is spontaneous and favourable. The positive value of  $\Delta H^\circ$  indicates that the adsorption process is endothermic in nature. The positive value of  $\Delta S^\circ$  indicates the increased randomness at the solid–solution interface during the adsorption of  $\text{Cu}^{2+}$ ,  $\text{Pb}^{2+}$  and  $\text{Ni}^{2+}$  on Alg-Cys-MMT bio-nanocomposite.

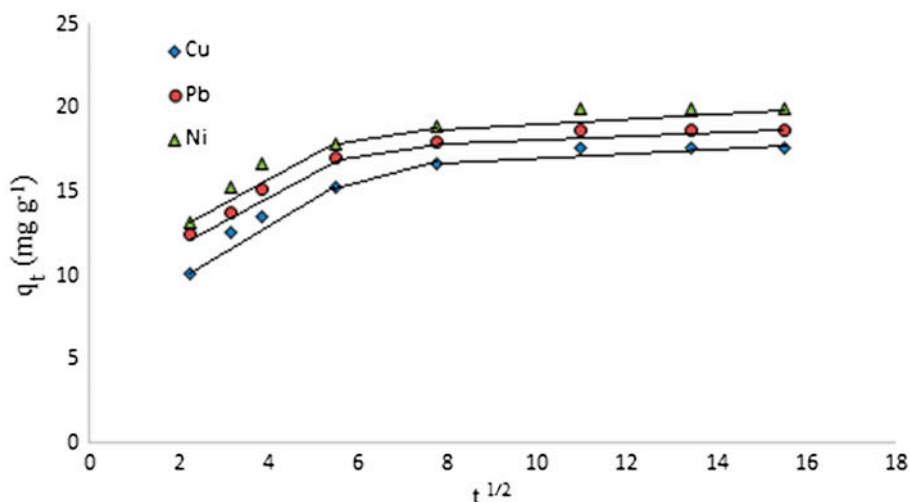


Fig. 17. Intraparticle diffusion model for the adsorption of  $\text{Cu}^{2+}$ ,  $\text{Pb}^{2+}$  and  $\text{Ni}^{2+}$  onto Alg-Cys-MMT nanocomposite with initial concentration ( $C_0 = 50 \text{ mg L}^{-1}$ ) and optimum pH of each metal ion at 25°C.

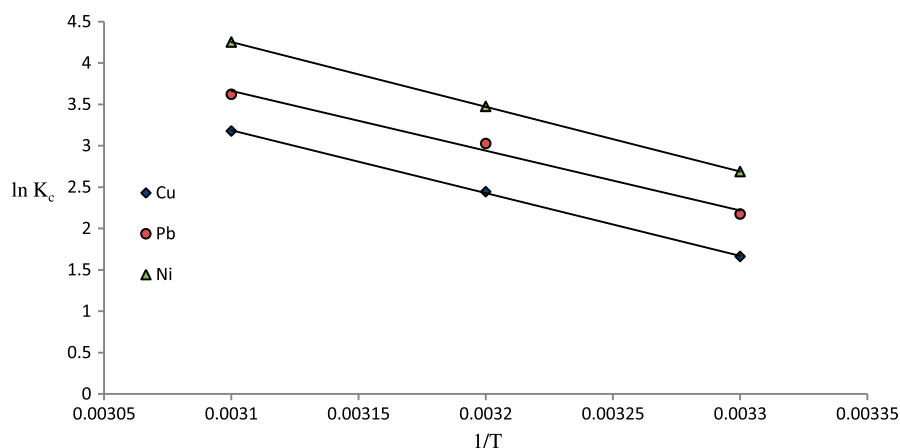


Fig. 18. Thermodynamic plot between  $\ln K_c$  and  $1/T$  at 30, 40 and 50°C for the adsorption of  $\text{Cu}^{2+}$ ,  $\text{Pb}^{2+}$  and  $\text{Ni}^{2+}$  onto Alg-Cys-MMT nanocomposite.

Table 3

Thermodynamic parameters for the adsorption of  $\text{Cu}^{2+}$ ,  $\text{Pb}^{2+}$  and  $\text{Ni}^{2+}$  onto Alg-Cys-MMT nanocomposite at 30, 40 and 50°C

Metals	Temperature (K)	$\Delta G^\circ$ (kJ mol <sup>-1</sup> )	$\Delta H^\circ$ (kJ mol <sup>-1</sup> )	$\Delta S^\circ$ (J mol <sup>-1</sup> K <sup>-1</sup> )
$\text{Cu}^{2+}$	303	-4.19	63.02	221.82
	313	-6.41		
	323	-8.63		
$\text{Pb}^{2+}$	303	-5.57	60.15	216.91
	313	-7.74		
	323	-9.91		
$\text{Ni}^{2+}$	303	-6.75	65.09	237.12
	313	-9.12		
	323	-11.49		

Table 4

Comparison of adsorption capacities (mg g<sup>-1</sup>) with other adsorbents

Adsorbent	$\text{Cu}^{2+}$	$\text{Pb}^{2+}$	$\text{Ni}^{2+}$	Refs.
Cross-linked alginate beads	54.90	–	–	[35]
Carbon nanotube/CA	67.9	–	–	[36]
Graphite carbon/CA	–	460.9	93.3	[37]
PSC	–	57.6	–	[38]
Magnetic alginate	–	–	30.49	[39]
Alginate beads	30.51	227.92	7.62	[40]
Silica/alginate	–	83.33	–	[41]
Alg-Cys-MMT	100.00	111.11	125.00	This study

### 3.8. Comparison of adsorption capacities

Table 4 demonstrates the comparison of adsorption capacity of various adsorbents. It is evident from the

table that the present adsorbent exhibits highest adsorption capacity towards all the metal ions. Therefore, the nanocomposite material can be successfully utilized for the removal of these metal ions.

#### 4. Conclusions

In this study, a biopolymer-based nanocomposite Alg-Cys-MMT was successfully synthesized and was characterized by various techniques such as XRD, FTIR, TGA-DTG, SEM and TEM. The nanocomposite was used in the removal of  $\text{Cu}^{2+}$ ,  $\text{Pb}^{2+}$  and  $\text{Ni}^{2+}$  from their aqueous solutions by batch method. However, the results obtained from the adsorption isotherm investigation indicated the data are best fitted to the Langmuir model in the concentration range studied. The  $q_m$  ( $\text{mg g}^{-1}$ ) from Langmuir model was found to be 125.0, 111.11 and 100.0  $\text{mg/g}$  for  $\text{Ni}^{2+}$ ,  $\text{Pb}^{2+}$  and  $\text{Cu}^{2+}$ , respectively, at a temperature of  $50^\circ\text{C}$  and optimum pH values corresponding to each metal ion. High pH and temperature values were found as the favourable conditions for maximum adsorption. The values of the thermodynamic parameters revealed that the adsorption of heavy metal ions onto Alg-Cys-MMT is spontaneous and endothermic in nature. Kinetics of adsorption was best followed by pseudo-second-order model.

#### Acknowledgements

The authors gratefully acknowledge the instrumentation laboratory, centre for excellence in nanomaterials, Department of Applied Physics, AMU, Sophisticated Analytical Instrumentation Facility (SAIF), Punjab University, Chandigarh, STIC, Cochin University, and highly thankful to UGC-MANF, Delhi, for providing financial assistance.

#### References

- [1] S.Q. Zhang, W.G. Hou, Adsorption behavior of Pb(II) on montmorillonite, *Colloids Surf., A* 320 (2008) 92–97.
- [2] M.Q. Jiang, X.Y. Jin, X.Q. Lu, Z.L. Chen, Adsorption of Pb(II), Cd(II), Ni(II) and Cu(II) onto natural kaolin clay, *Desalination* 252 (2010) 33–39.
- [3] J.P. Chen, L. Wang, Characterization of metal adsorption kinetic properties in batch and fixed-bed reactors, *Chemosphere* 54 (2004) 397–404.
- [4] A. Sari, M. Tuzen, O.D. Uluözlü, M. Soylak, Biosorption of Pb(II) and Ni(II) from aqueous solution by lichen (*Cladonia furcata*) biomass, *Biochem. Eng. J.* 37 (2007) 151–158.
- [5] A.A. Atia, A.M. Donia, A.M. Yousif, Removal of some hazardous heavy metals from aqueous solution using magnetic chelating resin with iminodiacetate functionality, *Sep. Purif. Technol.* 61 (2008) 348–357.
- [6] K. Yamashiro, K. Miyoshi, R. Ishihara, D. Umeno, K. Saito, T. Sugo, S. Yamada, H. Fukunaga, M. Nagai, High-throughput solid-phase extraction of metal ions using an iminodiacetate chelating porous disk prepared by graft polymerization, *J. Chromatogr. A* 1176 (2007) 37–42.
- [7] R. Ahmad, R. Kumar, M.A. Laskar, Adsorptive removal of  $\text{Pb}^{2+}$  from aqueous solution by macrocyclic calyx [4]naphthalene: Kinetic, thermodynamic, and isotherm analysis, *Environ. Sci. Pollut. Res.* 20 (2013) 219–226.
- [8] R. Ahmad, R. Kumar, Conducting polyaniline/iron oxide composite: a novel adsorbent for the removal of Amido Black 10 B, *J. Chem. Eng. Data* 55 (2010) 3489–3493.
- [9] A.F. Ngomsik, A. Bee, J.M. Siaugue, V. Cabuil, G. Cote, Nickel adsorption by magnetic alginate microcapsules containing an extractant, *Water Res.* 40 (2006) 1848–1856.
- [10] H. Mittal, S.B. Mishra, Gum ghatti and  $\text{Fe}_3\text{O}_4$  magnetic nanoparticles based nanocomposites for the effective adsorption of Rhodamine B, *Carbohydr. Polym.* 101 (2014) 1255–1264.
- [11] N. Fedullo, E. Sorlier, M. Sclavons, C. Bailly, J. Lefebvre, J. Devaux, Polymer based nanocomposites: Overview, applications and perspectives, *Prog. Org. Coat.* 58 (2007) 87–95.
- [12] M.S. Smole, K. Stakne, K. Kleinschek, M. Kurecic, M. Bele, D. Svetec, Electrokinetic properties of polypropylene-layered silicate nanocomposite fibers, *J. Appl. Polym. Sci.* 113(2) (2009) 1276–1281.
- [13] S.S. Ray, M. Okamoto, Polymer/layered silicate nanocomposites: A review from preparation to processing, *Prog. Polym. Sci.* 28 (2003) 1539–1641.
- [14] K.G. Bhattacharyya, S.S. Gupta, Adsorption of a few heavy metals on natural and modified kaolinite and montmorillonite: A review, *Adv. Colloid Interface Sci.* 140 (2008) 114–131.
- [15] N. Öztürk, A. Tabak, S. Akgöl, A. Denizli, Reversible immobilization of catalase by using a novel bentonite–cysteine (Bent–Cys) microcomposite affinity sorbents, *Colloids Surf., A* 322 (2008) 148–154.
- [16] N. Öztürk, A. Tabak, S. Akgöl, A. Denizli, Newly synthesized bentonite–histidine (Bent–His) micro-composite affinity sorbents for IgG adsorption, *Colloids Surf., A* 301 (2007) 490–497.
- [17] M. Alboofetileh, M. Rezaei, H. Hosseini, M. Abdollahi, Effect of montmorillonite clay and biopolymer concentration on the physical and mechanical properties of alginate nanocomposite films, *J. Food Eng.* 117(1) (2013) 26–33.
- [18] G.V. Joshi, B.D. Kevadiya, H.A. Patel, H.C. Bajaj, R.V. Jasra, Montmorillonite as a drug delivery system: Intercalation and in vitro release of timolol maleate, *Int. J. Pharm.* 374 (2009) 53–57.
- [19] Y. Vijaya, S.R. Popuri, V.M. Boddu, A. Krishnaiah, Modified chitosan and calcium alginate biopolymer sorbents for removal of nickel(II) through adsorption, *Carbohydr. Polym.* 72 (2008) 261–271.
- [20] H. Min, J. Wang, H. Hui, W. Jie, Study on emulsion polymerization of PMMA/OMMT nanocomposites by redox initiation, *J. Macromol. Sci. Part B Phys.* 45 (2006) 623–629.
- [21] H. Li, Y. Yu, Y. Yang, Synthesis of exfoliated polystyrene/montmorillonite nanocomposite by emulsion polymerization using a zwitterion as the clay modifier, *Eur. Polym. J.* 41 (2005) 2016–2022.
- [22] S.S. Ray, M. Bousmina, Biodegradable polymers and their layered silicate nanocomposites: In greening the 21st century materials world, *Prog. Mater. Sci.* 50 (2005) 962–1079.

- [23] B. Lee, Y. Kim, Y. Lee, J. Yi, Synthesis of functionalized porous silica via tem-plating method as heavy metal ion adsorbents, the introduction of surface hydrophilicity onto the surface of adsorbents, *Microporous Mesoporous Mater.* 50 (2001) 77–90.
- [24] N. Unlu, M. Ersoz, Adsorption characteristics of heavy metal ions onto a low cost biopolymeric sorbent from aqueous solutions, *J. Hazard. Mater.* 136 (2006) 272–280.
- [25] A. Murugesan, L. Ravikumar, V. SathyaSelvaBala, P. SenthilKumar, T. Vidhyadevi, S. Dinesh Kirupha, Removal of Pb(II), Cu(II) and Cd(II) ions from aqueous solution using polyazomethineamides: Equilibrium and kinetic approach, *Desalination* 271 (2011) 199–208.
- [26] W. Shen, S. Chen, S. Shi, X. Li, X. Zhang, W. Hu, Adsorption of Cu(II) and Pb(II) onto diethylenetriamine-bacterial cellulose, *Carbohydr. Polym.* 75 (2009) 110–114.
- [27] R. Djeribi, O. Hamdaoui, Sorption of Cu(II) from aqueous solutions by cedar sawdust and crushed brick, *Desalination* 225 (2008) 95–112.
- [28] K.Y. Foo, B.H. Hameed, Insights into the modeling of adsorption isotherm systems, *Review. Chem. Eng. J.* 156 (2010) 2–10.
- [29] A.O. Dada, A.P. Olalekan, A.M. Olatunya, O. Dada, Langmuir, Freundlich, Temkin and Dubinin–Radushkevich isotherms studies of equilibrium sorption of  $Zn^{2+}$  unto phosphoric acid modified rice husk, *J. Appl. Chem.* 3 (2012) 38–45.
- [30] A.E. Ofomaja, E.B. Naidoo, S.J. Modise, Kinetic and pseudo-second-order modeling of lead bio-sorption onto pine cone powder, *Ind. Eng. Chem. Res.* 49 (2010) 2562–2572.
- [31] M. Monier, D.M. Ayad, A.A. Sarhan, Adsorption of Cu(II), Hg(II), and Ni(II) ions by modified natural wool chelating fibres, *J. Hazard. Mater.* 176 (2010) 348–355.
- [32] R.N. Goyal, A. Kumar, A. Mittal, Oxidation chemistry of adenine and hydroxyadenines at pyrolytic graphite electrodes, *J. Chem. Soc., Perkin Trans. II* 9 (1991) 1369–1375.
- [33] E.S.Z. El-Ashtoukhy, N.K. Amin, O. Abdel Wahab, Removal of lead(II) and copper(II) from aqueous solution using pomegranate peel as a new adsorbent, *Desalination* 223 (2008) 162–173.
- [34] Y.S. Ho, A. Ofomaja, Kinetics and thermodynamics of lead ion sorption on palm kernel fibre from aqueous solution, *Process Biochem.* 40 (2005) 3455–3461.
- [35] T. Lu, T. Xiang, X.L. Huang, C. Li, W.F. Zhao, Q. Zhang, C.S. Zhao, Post cross linking towards stimuli-responsive sodium alginate beads for the removal of dye and heavy metals, *Carbohydr. Polym.* 133 (2015) 587–595.
- [36] Y. Li, F. Liu, B. Xia, Q. Du, P. Zhang, D. Wang, Z. Wang, Y. Xia, Removal of copper from aqueous solution by carbon nanotube/calcium alginate composites, *J. Hazard. Mater.* 177 (2010) 876–880.
- [37] D.W. Cho, W. Jung, A. Sigdel, O.H. Kwon, S.H. Lee, A.N. Kabra, B.H. Jeon, Adsorption of Pb(II) and Ni(II) from aqueous solution by nanosized graphite carbon-impregnated calcium alginate bead, *Geosyst. Eng.* 16 (2013) 200–208.
- [38] X. Ma, X. Liu, D.P. Anderson, P.R. Chang, Modification of porous starch for the adsorption of heavy metal ions from aqueous solution, *J. Food Chem.* 181 (2015) 133–139.
- [39] A.F. Ngomsik, A. Bee, J.M. Siaugue, V. Cabuil, G. Cote, Nickel adsorption by magnetic alginate microcapsules containing an extractant, *Water Res.* 40 (2006) 1848–1856.
- [40] B. An, H. Lee, S. Lee, S.H. Lee, J.W. Choi, Determining the selectivity of divalent metal cations for the carboxyl group of alginate hydrogel beads during competitive sorption, *J. Hazard. Mater.* 298 (2015) 11–18.
- [41] R.D.C. Soltani, A.R. Khataee, S. Jorfi, Silica nanopowders/alginate composite for adsorption of lead(II) ions in aqueous solutions, *J. Taiwan Inst. Chem. Eng.* 45 (2014) 973–980.